In vivo selective imaging of metabolic glycosylation with a tetrazine-modified upconversion nanoprobe†

Ruijing Zhang,[ab] Judun Zheng[*ab] and Tao Zhang [ID] [*ab]

Glycans play an important role in various physiological and pathological processes. Metabolic labeling with bioorthogonal chemistry is a distinguished tool for detecting and tracking glycans in cells and *in vivo*. However, most of the currently available bioorthogonal turn-on probes based on organic fluorophores still suffer from some inevitable deficiencies, including shallow tissue penetration and spontaneous fluorescence. Herein, we designed and reported a bioorthogonal turn-on nanoprobe UCNP-T, which could realize the specific labeling and visualization of glycans on living cell membranes. UCNP-T was constructed based on a multi-spectral upconversion nanophosphor (UCNP) as the luminescence resonance energy transfer (LRET) donor and an organic molecule, tetrazine, as the acceptor. Using the as-prepared UCNP-T, we could specifically label the cell-surface glycans and monitor their level in living mice in real time through the ratio of upconversion luminescence (UCL) emissions of 540 nm to 650 nm (UCL_{540}/UCL_{650}), providing sensing with highly intrinsic reliability by self-calibration. Thus, the nanoprobe would provide a reliable tool for elucidating the role of glycosylation in cells and *in vivo*.

Introduction

Glycans, a family of biological macromolecules mainly existing in glycoproteins or glycolipids, play a vital role in diverse biological and pathological processes.[1–3] Dysregulation of glycosylation, for example that observed for polysialic acid (PSA), is widely regarded as an implicated feature of numerous cancers.[4] Therefore, the visualization of glycosylation to understand various biological events has been of great importance.[5] Subsequently, abundant advances based on genetic methodologies have been achieved, but they need a long period.[6,7] Recently, the metabolic glycan labeling technique, which takes advantage of the underlying biosynthetic machinery to metabolically incorporate an unnatural sugar analogue into cell-surface glycans, has emerged as an attractive protocol for detecting and imaging glycans in live cells and living animals.[8–11] Generally, cells are first fed with non-natural monosaccharides modified with bioorthogonal functional groups, such as azide, alkynyl cyclopropene and cycloalkane, to

metabolically afford cell-surface glycans with functional groups.[12–18] Subsequently, a fluorogenic imaging probe carrying a complementary functional group can specifically recognize the cell-surface glycans *via* a bioorthogonal reaction. Fluorescence optical imaging based on organic dyes has provided valuable information about glycans; however, these organic probes are susceptible to several interferences including their tendency towards photobleaching, tissue autofluorescence and small penetration depth by UV/visible excitation light sources.

Multi-spectral lanthanide-doped upconversion nanoparticles (UCNPs) that can convert continuous-wave near-infrared (NIR) excitation to visible emission have been recognized as an alternative candidate for labeling and monitoring the target of interest. UCNPs exhibit outstanding photophysical features including high photostability, remarkable light penetration depth, long life and tunable multi-color emissions,[19–22] due to which they can be regarded as promising energy donors for luminescence resonance energy transfer (LRET)-based nanoprobes.[23–25] Accordingly, the combination of UCNPs with organic fluorescent sensors has gained great results in biolabeling and biosensing *via* the target-induced recovery of UCNP luminescence.[26–32] Therefore, the construction of an LRET-based upconversion nanoprobe for the specific labeling and real-time imaging of glycans can provide a promising prospect for obtaining a high-intensity signal and imaging of the cell membrane.

Herein, we developed an LRET-based bioorthogonal nanoprobe, UCNP-T, for the metabolic labeling and real-time imaging of cell-surface glycans (Fig. 1). Specifically, the cell-specific

*a*MOE Key Laboratory of Laser Life Science & Institute of Laser Life Science, College of Biophotonics, South China Normal University, Guangzhou, China. E-mail: zt@scnu.edu.cn

*b*Guangdong Provincial Key Laboratory of Laser Life Science, College of Biophotonics, South China Normal University, Guangzhou, China

† Electronic supplementary information (ESI) available: Absorbance spectra of tetrazine, UCNP, UCNP-T in the absence or presence of TCO; DLS result of UCNP and UCNP-T; dark toxicity of UCNP-T; ¹H NMR and ESI-MS spectrum of $Ac_4ManNTCO$; UCL imaging of glycans status in the tumor-bearing mice pretreated Ac_4ManNH_2. See DOI: 10.1039/d0ra01832e
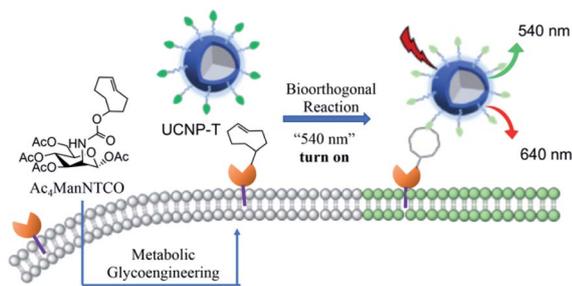
Paper

Fig. 1 Schematic of cell membrane ratiometric UCF detection.

glycan labeling strategy employed a tetrazine-bearing nanoprobe to recognize the cells metabolically decorated with *trans*-cyclooctenol (TCO) groups *via* pre-treatment with peracetylated mannosamine (Ac$_4$ManNTCO). The nanoprobe UCNP-T could be facilely synthesized by covalently modifying the water-soluble UCNPs with tetrazine. We rationally chose tetrazine as the energy acceptor not only because it is a known bio-orthogonal counterpart but also because its absorption band (500–600 nm) overlaps well with the upconversion luminescence (UCL) emissions of the transition bands of Er^{3+} ($^2H_{11/2} \rightarrow$ $^4H_{15/2}$, 514–534 nm; $^4H_{3/2} \rightarrow$ $^4H_{15/2}$, 534–560 nm). The UCL of UCNP-T at 540 nm (UCL$_{540}$) was thereby quenched but that of UCNP-T at 650 nm (UCL$_{650}$) was uninterfereced. When UCNP-T was activated by TCO, the LRET between UCNP and tetrazine was blocked and resulted in the "turn-on" recovery of UCL$_{540}$. Based on this, we could use the ratio of UCL$_{540}$/UCL$_{650}$ as a ratiometric detection signal to achieve the selective and sensitive labeling and detection of the cell-surface glycans. Moreover, we demonstrated our probe as a reliable tool in recognizing and imaging specific glycans *in vivo*.

Experimental

Synthetic procedure of PEI-capped NaYF$_4$:Yb^{3+}, Er^{3+} (UCNPs)

Water-dispersed NaYF$_4$:Yb^{3+}, Er^{3+} nanoparticles were successfully prepared by a one-step hydrothermal method.[33] Generally, PEI (branched 25 kDa, 1 g), 1 mmol of NaCl, and 1 mmol of YCl$_3$ (0.5 mol L^{-1}), YbCl$_3$ (0.5 mol L^{-1}), and ErCl$_3$ (0.1 mol L^{-1}) with a molar ratio of 78 : 20 : 2 were dissolved in ethanol (20 mL) and stirred for 30 minutes. Then, 10 mL of ethanol containing 5.5 mmol of NH$_4$F was added to the above solution and stirred for another 30 min. The obtained mixture was transferred to a 50 mL stainless teflon-lined autoclave. The autoclave was sealed and kept at 190 °C for 24 h and then cooled to room temperature. The precipitate was then collected by centrifugation (9000 g, 5 min), washed with ethanol and deionized water several times and dried over vacuum at 60 °C for 12 h to afford the as-prepared NaYF$_4$:Yb^{3+}, Er^{3+} coated with PEI as a white powder.

Tetrazine modification of UCNPs (UCNP-T)

(4-(1,2,4,5-Tetrazin-3-yl)phenyl)-methanamine (tetrazine-benzylamine) was produced according to a previously reported method.[34] Tetrazine-benzylamine (10 mg, 0.05 mmol) and

succinic anhydride (10 mg, 0.01 mmol) were dissolved in methylene chloride (5 mL) and then, triethylamine (30 μL, 0.5 mmol) was added to this solution. The mixture was heated to 50 °C and then stirred for 18 h. After the reaction was complete, the solvent was removed under reduced pressure and water was poured into the remaining paste. Then, the pH of the solution was adjusted to 3.0 with hydrochloric acid to get a red product, which was collected by centrifugation. UCNPs (10 mg), EDC (24 mg, 1.5 mmol), NHS (16 mg, 1.5 mmol) and TCO (28 mg, 0.1 mmol) were mixed in DMF (5 mL) and stirred overnight at room temperature. After this, the crude product was added to saturated salt water and extracted with ethyl acetate. Then, pure UCNP-T was obtained after being dried over vacuum at 1 h.

Synthesis of Ac$_4$ManNTCO

Ac$_4$ManNH$_2$ was produced according to previous literature.[35] Ac$_4$ManNH$_2$ (3.48 mg, 0.01 mmol), TCO-NHS (2.68 mg, 0.01 mmol) and Et$_3$N (2 μL) were dissolved in dry methylene chloride (10 mL) under nitrogen. The mixture was stirred for 12 h at room temperature. The reaction mixture was collected with methylene chloride solution, dried with Na$_2$SO$_4$, and then concentrated. The crude product was purified over a silica gel column chromatograph with methanol/methylene chloride (1 : 20) as the eluent to afford the pure product Ac$_4$ManNTCO (3.58 mg, 71.6%). ^{1}H NMR (400 MHz, d_6-DMSO): 8.08 (d, $J = 8.0$ Hz, 1H), 6.13 (s, 2H), 5.74 (s, 1H), 5.41 (t, $J = 8$ Hz, 2H), 5.20 (d, $J = 8$ Hz, 2H), 5.18 (d, $J = 8$ Hz, 1H), 3.97–4.19 (m, 7H), 3.71 (d, $J = 4$ Hz, 1H), 2.16 (s, 1H), 2.03 (t, $J = 8$ Hz, 12H), 1.91 (s, 1H). ESI-MS (m/z): calculated for C$_{23}$H$_{33}$NO$_{11}$, 499.51 [M]; found, 499.8000.

Cytotoxicity assay *in vitro*

Relative cell viabilities were determined by the CCK-8 assay. EMT6 cells were seeded into 96-well plates at a density of 1×10^4 cells per well and incubated for 12 h at 37 °C, followed by incubation with different concentrations of UCNP-T solutions (0, 50, 100, 150, and 200 μM) for 24 h. Then, these cells were washed with PBS (pH 7.4) to remove the unbound compound, and a fresh culture medium was added. Then, CCK-8 (10 μL per well, 5 mg mL^{-1}) was added to each well and the plate was incubated for an additional 1 h at 37 °C under 5% CO$_2$. The absorbance of each well was measured at a wavelength of 450 nm using a microplate reader.

Confocal fluorescence imaging

First, EMT6 cells were pretreated with Ac$_4$ManNTCO (50 μM) for two days and washed with PBS (pH 7.4) twice. The cells were then incubated with UCNP-T (50 μM) for 2 h; the culture medium was washed with PBS and observed by CLSM. The images were obtained using an Olympus fluoview FV10 microscope. The luminescence of UCNP-T excited at 980 nm was recorded in the green and red channels.

Glycan imaging *in vivo*

All animal procedures were performed in accordance with the National Institutes of Health (NIH) Guidelines for the Care and

Use of Laboratory Animals of South China Normal University, and the experiments were approved by the Animal Ethics Committee of South China Normal University. The imaging study was started when tumors reached a size between 100 and 120 mm^3. The first group of mice was intratumorally injected with Ac$_4$ManNH$_2$ (0.2 mL, 50 μmol L^{-1}), the second group of mice was injected with the same concentration of Ac$_4$ManNTCO (0.2 mL, 50 μmol L^{-1}) in PBS, the third group of mice was injected with a lower concentration of Ac$_4$ManNTCO (0.2 mL, 30 μmol L^{-1}). After 3 days, all groups of mice were intravenously injected with 200 μL UCNP-T at the same concentration (50 μmol L^{-1}). Then, the UCL images of mice were recorded by a CCD camera with a 980 nm laser (0.5 W cm^{-2}) at different post times (0, 3, 6, 12 and 24 h).

Fig. 3 (A) UV-Vis spectra of tetrazine (black) together with the UCL spectrum of Yb^{3+}/Er^{3+}-codoped UCNP, nanoprobe UCNP-T and UCNP-T + TCO (green, red and blue). TEM images of UCNPs (B) and UCNP-T (C); scale bars are 20 nm.

Results and discussion

Construction and characterization of the nanoprobe UCNP-T

In this manuscript, Fig. 2 illustrates the synthetic route of the luminogenic terazine-based upconversion nanoparticles (UCNP-T) and presents the turn-on progress at UCL$_{540}$. To enhance the water dispersibility of the nanomaterials, 980 nm-excited UCNPs (NaYF$_4$:20% Yb^{3+}, 2% Er^{3+}) coated with branched poly(ethylenimine) (PEI), a polycationic amphiphilic polymer, were prepared by a one-step hydrothermal method according to the literature.[33,36] Then, the UCNPs were further covalently modified with a sufficient amount of tetrazine to obtain UCNP-T, which was used to label and image the cell-surface glycans *via* 980 nm excitation.

The synthesis of UCNP-T was first verified by UV-Vis absorption spectra. A new absorbance peak appeared at 540 nm, which corresponded to the typical absorption of tetrazine, indicating the successful decoration of tetrazine (Fig. S1†). The luminescence spectra of the as-prepared UCNP-T together with the UCNP solution were then recorded under the excitation of a 980 nm laser. As shown in Fig. 3A, UCNPs exhibit two typical emission bands centered at 540 and 650 nm. Remarkably, compared with the emission spectrum of UCNPs, the green UCL$_{540}$ emission of UCNP-T was suppressed dramatically, which can be caused by the LRET-induced quenching effect. With the addition of TCO targeted to UCNP-T, the absorbance peak significantly decreased but an enhancement in the green emission at 540 nm was recorded, indicating that the loss of tetrazine could lead to the recovery of the luminescence of UCNP-T (Fig. S1† and 3A). The recovery of luminescence was attributed to the low LRET efficiency from UCNP-T to tetrazine. With no changes in the red UCL$_{650}$ emission, we confirmed that UCL$_{650}$ could be used as an internal
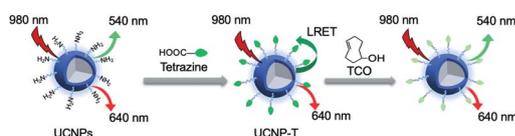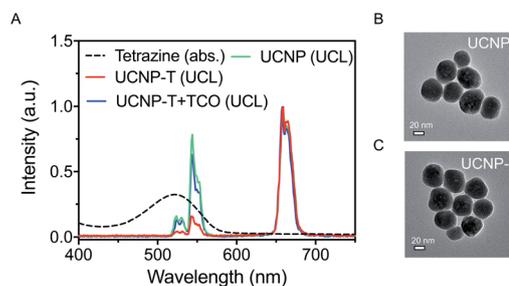
reference. Using the ratio of UCL$_{540}$/UCL$_{650}$ of the UCNP-T nanoprobe as a detection signal, simultaneous monitoring and imaging of glycans can be achieved *via* combining with metabolic glycan engineering.

Furthermore, transmission electron microscopy (TEM) revealed that UCNP-T exhibited uniform morphology and size with a diameter of ∼60 nm, indicating that no obvious changes were recorded in the size and shape of the nanoprobe after modification with tetrazine (Fig. 3B and C). UCNPs and UCNP-T have a similar hydrodynamic diameter of about ∼100 nm, as calculated from the analysis of the dynamic light scattering (DLS) results (Fig. S2†). Compared with the sizes observed *via* TEM, the significant increase in the hydrodynamic diameters is attributed to the dwelling effect of the polymer PEI.[37] Due to the modification of the water-soluble and biocompatible polymer, UCNP-T showed excellent stability in deionized water, which made it suitable for bioimaging applications. Taken together, these results confirmed that the water-soluble UCNP-T was successfully synthesized.

Sensing capability by UCNP-T for TCO

The quantitative analysis of UCNP-T for the detection of TCO was evaluated by using UV-Vis absorption and UCL emission spectroscopy techniques. As is known, the reaction of tetrazine and TCO is the fastest bioorthogonal transformation and can be applied to a variety of biological pursuits.[38–40] Based on the efficiency of LRET between tetrazine and UCNP-T, the typical absorption spectrum of tetrazine was investigated. After titration with different concentrations of TCO, the absorbance bands at 450–600 nm gradually decreased, indicating that a reaction between TCO and tetrazine occurred on the surface layer of UCNP-T (Fig. 4A). Moreover, a significant TCO-induced hypochromicity could be observed, and the value of absorbance at 540 nm (Abs$_{540}$) decreased linearly with a correlation factor of 0.9903 (Fig. 4B). The UCL sensing ability of UCNP-T for TCO was also monitored (Fig. 4C). Following the addition of TCO, the green UCL$_{540}$ emission of UCNP-T gradually recovered under 980 nm irradiation owing to the decreased efficiency of LRET from UCNP-T to tetrazine. Using the unaffected UCL$_{650}$ as an internal standard, a linear relationship between the ratio of

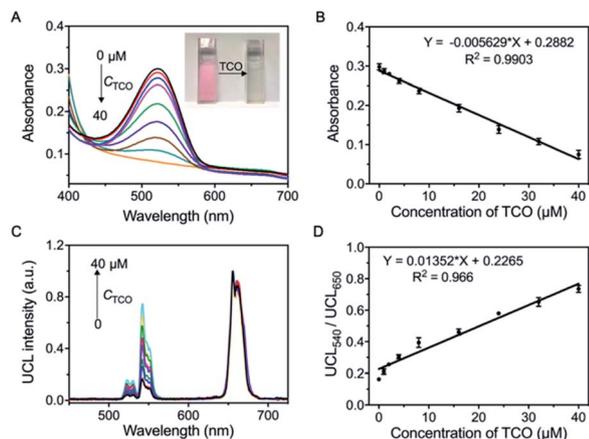Fig. 2 Synthesis of the upconversion nanoprobe (UCNP-T).

Fig. 4 (A) The absorbance spectra of UCNP-T in the absence or presence of TCO at different concentrations (inset: photograph of UCNP-T before and after incubation of TCO). (B) The plot of intensity of absorbance at 540 nm with a linear equation. (C) Upconversion luminescence spectra of 20 μM UCNP-T (PBS) with the gradual addition of TCO. (D) Plots of UCL_{540}/UCL_{650} of UCNP-T versus different concentrations of TCO.

UCL_{540}/UCL_{650} was found, which was in agreement with the above-mentioned absorption changes (Fig. 4D). Considering the above-mentioned results, UCNP-T can be used as a preferable tool with great turn-on luminescence behaviour for detecting analytes containing the TCO group.

UCNP-T monitoring of TCO-modified glycans in living cells

Having shown that the UCNP-T luminescence responded well to the TCO within a physiological environment, we next evaluated its ability to visualize specific biomolecules in living cells. Glycan-specific metabolic engineering is of special importance in various biological events, such as cell adhesion and cell recognition as well as inter-cellular and intracellular signaling; thus, the visualization of glycans is very meaningful.[41–43] Before exploring cellular labeling and bioimaging, the cytotoxicity of UCNP-T was investigated by a Cell Counting Kit-8 (CCK-8) assay. The mouse mammary cells (EMT6) viabilities were all higher than 93% with different probe doses (0–200 μM) for 24 h (Fig. S3†), suggesting that UCNP-T has less toxicity and good biocompatibility.

Considering the importance of cell-surface glycans in diverse biological and pathological processes, we employed Ac4-ManNTCO to metabolically modify the corresponding sialylated glycans with TCO groups on the cell surface for the subsequent glycan labeling through bioorthogonal conjugation. The rapid kinetics of tetrazine-based bioorthogonal reactions, which are referred to as inverse electron-demand Diels–Alder reactions between tetrazine and diverse dienophiles,[38] ensure efficient Ac4ManNTCO–tetrazine bioorthogonal labeling even at low concentrations. Moreover, the bioorthogonal Ac4ManNTCO–tetrazine labeling could occur inside the living systems without interfering with the native biochemical processes. Therefore, using the Ac4ManNTCO–tetrazine pair for glycan labeling can be an excellent strategy for the sensitive and selective detection of glycomes in living cells and in vivo.

The per-acetylated mannosamine-decorated TCO group via amido bonds (Ac4ManNTCO) was successfully synthesized and characterized by ^{1}H NMR spectroscopy and ESI-MS (Fig. S4 and S5†). After metabolic oligosaccharide engineering (MOE), the TCO group which was modified and labeled in the sialic acid monosaccharide via a biosynthetic pathway was successfully incorporated into the cell surface. In order to label the glycans present in cells, EMT6 cells were treated with Ac4ManNTCO (50 μM) for 2 days to metabolically convert them into the corresponding O-linked sialylated glycans bearing TCO groups on the cell surface. Then, the Ac4ManNTCO-pretreated EMT6 cells were incubated with 50 μM UCNP-T. To verify the sensing capability of UCNP-T, real-time fluorescence imaging was performed by a fluorescence microscope equipped with a 980 nm laser. As displayed in Fig. 5, the cells show very weak green emission at 540 nm after 0.25 h, while significant red emission at 650 nm is observed within this region. As the time went on, the intensity of UCL_{540} increased substantially following post-incubation at 2 h, and a slight enhancement in the intensity of UCL_{650} was observed.

It is a remarkable fact that the ratiometric detection and imaging method is more precise and important than those with single luminescence signals in the detection of tumor biomarkers because it can avoid the effects of instrumental efficiency, environmental conditions, and nanoprobe concentration. Under 980 nm laser excitation, considering the obvious enhancement in the green UCL_{540} emission and the unaffected red UCL_{650} emission of UCNP-T, the ratiometric UCL imaging was further demonstrated by recording the luminescence at the green channel (525–575 nm) and red channel (645–675 nm). A low UCL_{540}/UCL_{650} ratio was observed for the Ac4ManNTCO-preincubated cells treated with UCNP-T for 0.25 h, while the corresponding UCL ratio increased to 0.88 after 2 hours (Fig. S6†). The results suggested that UCNP-T could be used for monitoring the cell-surface Ac4ManNTCO with the ratiometric UCL method.

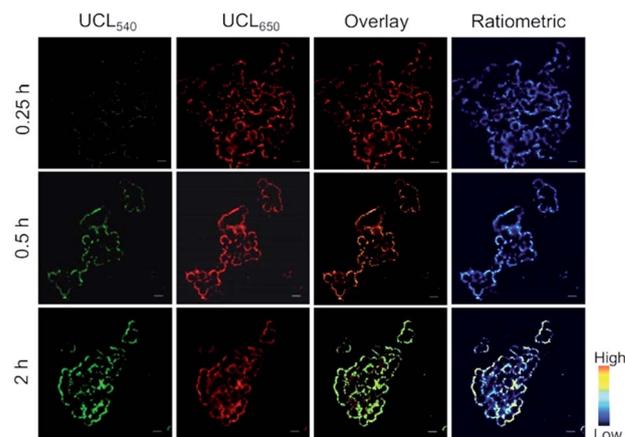Fig. 5 Intracellular ratiometric upconversion images of EMT6 cells pretreated with Ac4ManNTCO (50 μM) for two days and further incubation with UCNP-T (50 μM). Ratiometric UCL confocal microscopy images collected by green channel (UCL_{540}) and red channel (UCL_{650}) of EMT6 cells after being incubated with UCNP-T under 980 nm excitation. Scale bar: 20 μm.

UCL real-time monitoring and imaging of glycans *in vivo*

As previously reported, the altered glycosylation of cell surface proteins is an important indicator of tumor phenotypes. In particular, during metastatic invasion and tumor progression, the cancer cells can affect the way the cancer cells interact with the extracellular matrix, neighbouring cells and the epithelium of the target organ.[44,45] As an activatable detector, the nanoprobe UCNP-T was used to evaluate the TCO-modified glycans in a xenograft model of a living mouse. Based on the above-mentioned photophysical behaviour of UCNP-T, UCL_{650} could be used as a signal for monitoring the delivery of the nanoprobe in living mice.

Considering the possible limited tumor accumulating efficiency of the small molecular $Ac_4ManNTCO$ and that intratumoral injection is also commonly used in two-step chemical tumor-targeting systems,[46–48] herein, we chose intratumoral administration to selectively introduce sufficient TCO groups into tumor tissues. First, the EMT6 tumor-bearing BALB/c mice were pre-injected intratumorally with $Ac_4ManNTCO$ (200 μL, 50 μM) or Ac_4ManNH_2 (200 μL, 50 μM) for 3 days. After the tail intravenous injection of UCNP-T, the UCL images of the tumor region were recorded at various time points of 0, 3, 6, 12 and 24 h under the excitation of a 980 nm laser. As shown in Fig. S7,† the UCL_{650} intensity in the tumor region pretreated with Ac_4ManNH_2 was found to reach a relatively high level within 3 to 6 h through the enhanced permeability and retention (EPR) effect, while UCL_{540} was still maintained at a lower level with no obvious changes in the UCL_{540}/UCL_{650} ratio in these mice. Compared to the image obtained for the group pretreated with Ac_4ManNH_2, a brighter UCL image at 650 nm was recorded for the mice pretreated with $Ac_4ManNTCO$. The UCL_{650} signal intensity in the tumor sites increased and was maintained at a comparatively high level with the extension of time (Fig. 6A and B). Notably, a very sharp luminescence signal at 540 nm in the same region was also observed and showed the trend of increasing rapidly at first and then decreasing slowly, which could be attributed to the

biorthogonal binding reaction with the "receptor-like" glycans after selective accumulation in tumors. Furthermore, the UCL_{540}/UCL_{650} ratio for the mice pretreated with $Ac_4ManNTCO$ increased by 3-fold relative to that for the Ac_4ManNH_2-treated group post-injection for 6 h (Fig. 6C and S7†), indicating that TCO-labeled glycans were decorated on the cell surface *via* metabolic engineering. Meanwhile, labeling with a lower concentration of Ac_4-ManNTCO (30 μM, 200 μL) was also performed. As shown in Fig. S8,† the ratio of UCL_{540}/UCL_{650} presents a similar trend with a slight decrease compared with that for the $Ac_4ManNTCO$ (50 μM) injection, indicating that this strategy has good feasibility at different TCO-labeled glycan levels. Taken together, these results have demonstrated that UCNP-T can be used as an effective luminogenic probe for monitoring TCO-labeled glycomes in living mice.

Conclusions

LRET-based nanoprobes with upconversion nanoparticles as donors and organic molecules as acceptors have been of interest for the detection and imaging of cells, but the low LRET efficiency is still a substantial obstacle for sensitive detection. In order to improve the efficiency of energy transfer, two main factors need to be noted: the emission spectrum of the upconversion nanoparticles and the absorption spectrum of the organic molecules must overlap well; the spatial distance between the donor and the acceptor must be close enough. In this paper, since the 980 nm-excited UCNPs exhibited two typical emission bands centered at 540 and 650 nm, we selected tetrazine as the acceptor, which has a typical absorbance peak at 540 nm. Meanwhile, in order to reduce the distance and increase the loading efficiency of tetrazine, UCNPs were modified with amino-rich PEI to ensure that more tetrazine molecules combined with UCNPs to improve the efficiency of LRET.

In conclusion, we have designed and constructed a highly sensitive nanoprobe UCNP-T as a luminogenic bioorthogonal tool for the accurate ratiometric detection of cell-surface glycans. This nanoprobe was successfully established by attaching the tetrazine groups onto the surface of UCNPs. The probe presented weak emission of UCL_{540} due to the LRET from UCNP-T to tetrazine. The specific UCL_{540} emission enhancement was achieved *via* a bioorthogonal reaction between the tetrazine groups and *trans*-cyclooctene. The nanoprobe was identified as a reliable bioorthogonal tool for labelling specific *trans*-cyclooctene-modified glycans in living cells and mice by UCL bioimaging. Overall, the UCL-based nanoprobe for sensing and bioimaging glycans has potential for the *in vivo* diagnosis of glycan-related diseases.

Conflicts of interest

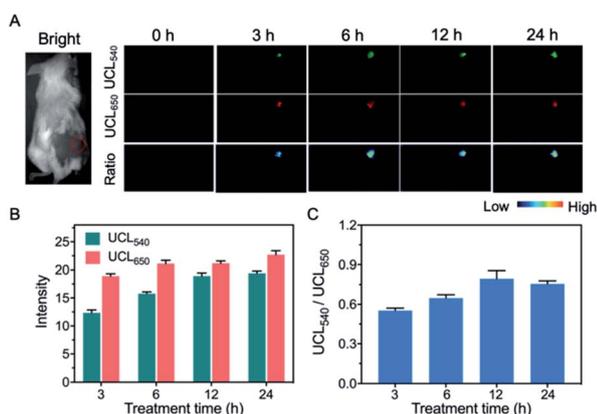There are no conflicts to declare.

Acknowledgements

Fig. 6 *In vivo* UCL imaging of glycans in tumors using UCNP-T. (A) Images of the tumor-bearing mice pretreated with $Ac_4ManNTCO$ for 3 days by the intratumor injection, followed by tail intravenous injection of UCNP-T (50 μM). The pseudo-colored bar represents the intensity of UCL_{540}, UCL_{650} and UCL_{540}/UCL_{650}. (B) The intensity of the UCL emission UCL_{540} and UCL_{650} of (A). (C) Quantified ratios of UCL_{540}/UCL_{650} intensity of (A).

Notes and references

1 Y. A. Wainman, A. A. Neves, S. Stairs, H. Stöckmann, H. I. Zecchini, K. M. Brindle and F. J. Leeper, *Org. Biomol. Chem.*, 2013, **11**, 7297–7300.

2 R. Xie, S. Hong, L. Feng, J. Rong and X. Chen, *J. Am. Chem. Soc.*, 2012, **134**, 9914–9917.

3 M. M. Fuster and J. D. Esko, *Nat. Rev. Cancer*, 2005, **5**, 526–542.

4 P. V. Chang, X. Chen, C. Smyrniotis, A. Xenakis, T. Hu, C. R. Bertozzi and P. Wu, *Angew. Chem., Int. Ed.*, 2009, **48**, 4030–4033.

5 P. W. Pan, Q. Zhang, J. Hou, Z. Liu, F. Bai, M. R. Cao, T. Sun and G. Bai, *Anal. Bioanal. Chem.*, 2012, **403**, 1661–1670.

6 A. Shajahan, S. Parashar, S. Goswami, S. M. Ahmed, P. Nagarajan and S. G. Sampathkumar, *J. Am. Chem. Soc.*, 2017, **139**, 693–700.

7 K. Ohtsubo and J. D. Marth, *Cell*, 2006, **126**, 855–867.

8 J. Rong, J. Han, L. Dong, Y. Tan, *et al.*, *J. Am. Chem. Soc.*, 2014, **136**, 17468–17476.

9 S. T. Laughlin, J. M. Baskin, S. L. Amacher and C. R. Bertozzi, *Science*, 2008, **320**, 664–667.

10 D. Rabuka, S. C. Hubbard, S. T. Laughlin, S. P. Argade and C. R. J. Bertozzi, *J. Am. Chem. Soc.*, 2006, **128**, 12078–12079.

11 J. A. Prescher, D. H. Dube and C. R. Bertozzi, *Nature*, 2004, **430**, 873–877.

12 C. P. Ramil and Q. Lin, *Chem. Commun.*, 2013, **49**, 11007–11022.

13 K. Lang and J. W. Chin, *Chem. Rev.*, 2014, **114**, 4764–4806.

14 B. Cheng, R. Xie, L. Dong and X. Chen, *ChemBioChem*, 2016, **17**, 11–27.

15 Y. Yuan, S. Xu, X. Cheng, X. Cai and B. Liu, *Angew. Chem., Int. Ed.*, 2016, **55**, 6457–6461.

16 J. Yang, J. Šečkutė, C. M. Cole and N. K. Devaraj, *Angew. Chem., Int. Ed. Engl.*, 2012, **51**, 7476–7479.

17 S. Stairs, A. A. Neves, H. Stöckmann, Y. A. Wainman, H. Ireland-Zecchini, K. M. Brindle and F. J. Leeper, *ChemBioChem*, 2013, **14**, 1063–1067.

18 A. Niederwieser, A. K. Späte, L. D. Nguyen, C. Jüngst, W. Reutter and V. Wittmann, *Angew. Chem., Int. Ed. Engl.*, 2013, **52**, 4265–4268.

19 D. K. Chatteriee, A. J. Rufalah and Y. Zhang, *Biomaterials*, 2008, **29**, 937–943.

20 Q. Liu, T. S. Yang, W. Feng and F. Y. Li, *J. Am. Chem. Soc.*, 2012, **134**, 5390–5397.

21 L. Q. Xiong, Z. G. Chen, Q. W. Tian, T. Y. Cao, C. J. Xu and F. Y. Li, *Anal. Chem.*, 2009, **81**, 8687–8694.

22 Q. Liu, Y. Sun, T. S. Yang, W. Feng, C. G. Li and F. Y. Li, *J. Am. Chem. Soc.*, 2011, **133**, 17122–17125.

23 Z. Li, S. W. Lv, Y. L. Wang, S. Y. Chen and Z. H. Liu, *J. Am. Chem. Soc.*, 2015, **137**, 3421–3427.

24 Y. S. Fenga, Y. N. Wua, J. Zuo, L. P. Tu, I. Que, Y. L. Chang, L. J. Cruzc, A. Chan and H. Zhang, *Biomaterials*, 2019, **201**, 33–41.

25 L. M. Yao, J. Zhou, J. L. Liu, W. Feng and F. Y. Li, *Adv. Funct. Mater.*, 2012, **22**, 2667–2672.

26 J. D. Zheng, Y. X. Wu, D. Xing and T. Zhang, *Nano Res.*, 2019, **12**, 931–938.

27 Q. W. Guo, Y. X. Liu, Q. Jia, G. Zhang, H. M. Fan, L. D. Liu and J. Zhou, *Anal. Chem.*, 2017, **89**, 4986–4993.

28 Z. H. Li, H. Yuan, W. Yuan, Q. Q. Su and F. Y. Li, *Chem. Rev.*, 2018, **354**, 155–168.

29 N. N. Wang, X. Y. Yu, K. Zhang, C. A. Mirkin and J. S. Li, *J. Am. Chem. Soc.*, 2017, **139**, 12354–12357.

30 J. K. Ni, C. X. Shan, B. Li, L. M. Zhang, H. P. Ma, Y. S. Luo and H. Song, *Chem. Commun.*, 2015, **51**, 14054–14056.

31 Y. X. Liu, Q. Jia, Q. W. Guo, A. Q. Jiang and J. Zhou, *Anal. Chem.*, 2017, **89**, 12299–12305.

32 J. J. Peng, A. Samanta, X. Zeng, S. Y. Han, L. Wang, D. D. Su, D. T. B. Loong, N. Y. Kang, S. J. Park and A. H. All, *Angew. Chem., Int. Ed.*, 2017, **56**, 4165–4169.

33 Q. W. Ding, Q. Q. Zhang, X. M. Zhou, T. Zhang and D. Xing, *Small*, 2016, **12**, 5944–5953.

34 H. S. Han, N. K. Devaraj, J. Lee, S. A. Hilderbrand, R. Weissleder and M. G. Bawendi, *J. Am. Chem. Soc.*, 2010, **132**, 7838–7839.

35 B. Cheng, R. Xie, L. Dong and X. Chen, *ChemBioChem*, 2015, **17**, 11–27.

36 F. Wang and X. G. Liu, *J. Am. Chem. Soc.*, 2008, **130**, 5642–5643.

37 J. Jin, Y. J. Gu, C. W. Y. Man, J. Cheng, Z. Xu, Y. Zhang, H. Wang, V. H.-Yi. Lee, S. H. Cheng and W. T. Wong, *ACS Nano*, 2011, **5**, 7838–7847.

38 D. M. Patterson, L. A. Nazarova and J. A. Prescher, *ACS Chem. Biol.*, 2014, **9**, 592–605.

39 D. M. Patterson, L. A. Nazarova, B. Xie, D. N. Kamber and J. A. Prescher, *J. Am. Chem. Soc.*, 2012, **134**, 18638–18643.

40 J. Yang, J. Seckute, C. M. Cole and N. K. Devaraj, *Angew. Chem., Int. Ed.*, 2012, **51**, 7476–7479.

41 A. Shajahan, S. Parashar, S. Goswami, S. M. Ahmed, P. Nagarajan and S. G. Sampathkumar, *J. Am. Chem. Soc.*, 2017, **139**, 693–700.

42 P. Pan, Q. Zhang and J. Hou, *Anal. Bioanal. Chem.*, 2012, **403**, 1661–1670.

43 H. Mçller, V. Bçhrsch, J. Bentrop, J. Bender, S. Hinderlich and P. R. Hackenberger, *Angew. Chem., Int. Ed.*, 2012, **51**, 5986–5990.

44 H. Wang, R. Wang, K. Cai, H. He, Y. Liu, J. Yen, Z. Y. Wang, M. Xu, Y. W. Sun, X. Zhou, Q. Yin, L. Tang, I. T. Dobrucki, L. W. Dobrucki, E. J. Chaney, S. A. Boppart, T. M Fan, S. Lezmi, X. S. Chen, L. C. Yin and J. J. Cheng, *Nat. Chem. Biol.*, 2017, **13**, 415–424.

45 R. Xie, L. Dong, R. B. Huang, S. L. Hong, R. X. Lei and X. Chen, *Angew. Chem., Int. Ed.*, 2014, **126**, 14306–14310.

46 H. Wang, M. Gauthier, J. R. Kelly, R. J. Miller, M. Xu, W. D. O'Brien Jr and J. Cheng, *Angew. Chem., Int. Ed.*, 2016, **55**, 5452–5456.

47 H. Koo, S. Lee, J. H. Na, S. H. Kim, S. K. Hahn, K. Choi, I. C. Kwon, S. Y. Jeong and K. Kim, *Angew. Chem., Int. Ed.*, 2012, **51**, 11836–11840.

48 H. Wang, L. Tang, Y. Liu, I. T. Dobrucki, L. W. Dobrucki, L. Yin and J. Cheng, *Theranostics*, 2016, **6**, 1467–1476.